A

$\mathtt{i^2tag}$: RFID Mobility and Activity Identification through Intelligent Profiling

Xiaoyi Fan, Simon Fraser University
Wei Gong, Simon Fraser University
Jiangchuan Liu, Simon Fraser University

Many Radio Frequency Identification (RFID) applications, e.g., virtual shopping-cart and tag-assisted gaming, involve sensing and recognizing tag mobility. Existing RFID localization methods however are mostly designed for static or slowly moving targets (less than 0.3 m/s). More importantly, we observe that prior methods suffer from serious performance degradation for detecting realworld moving tags in typical indoor environments with multipath interference. In this paper, we present $\mathtt{i^2tag}$, an intelligent mobility-aware activity identification system for RFID tags in multipath-rich environments, e.g., indoors. $\mathtt{i^2tag}$ employs a supervised learning framework based on our novel fine-grained *mobility profile*, which can quantify different levels of mobility. Unlike previous methods that mostly rely on phase measurement, $\mathtt{i^2tag}$ takes into account various measurements, including RSSI variance, packet loss rate, and our novel relative-phase-based fingerprint. Additionally, we design a *multiple dimensional dynamic time warping* based algorithm to robustly detect mobility and the associated activities. We show that $\mathtt{i^2tag}$ is readily deployable using off-the-shelf RFID devices. A prototype has been implemented using a `Thingmagic` reader and standard-compatible tags. Experimental results demonstrate its superiority in mobility detection and activity identification in various indoor environments.

CCS Concepts:•**Networks** → **Network mobility; Sensor networks;**•**Computer systems organization** → **Sensor networks;**

Additional Key Words and Phrases: RFID, Backscatter, Mobility Detection, Activity Identification

1. INTRODUCTION

The past few years have seen booming interest in human activity identification that provides a range of Internet-of-Things applications, such as healthcare and smart homes [Alam et al. 2012]. Traditional solutions mainly use radars [Xiao et al. 2016], cameras [Chaquet et al. 2013], and various inertial sensors [Bulling et al. 2014]. Yet, sensor or device based radar solutions require targets carrying sensors/wireless devices that are often not negligible in both size and weight. While camera-based and device-free radar-based systems have freed this limitation, they suffer poor performance in accurately identifying multiple objects, especially under Non-Line-of-Sight (NLoS) scenarios. Radio Frequency Identification (RFID) is a promising technology that can overcome those difficulties due to its low cost, small form size, and batterylessness, making it widely used in a range of mobile applications. For example, IKEA Canada has completed a solution that enables shoppers to purchase merchandise with the tap of a spoon that has a built-in tag, freeing shoppers from having to push carts or carry baskets around the store[1]. Disney has built an RFID gaming system that can sense when the player is moving or touching objects attached with tags in near real time [Spielberg et al. 2016].

The mobility of targets is an essential and important metric to differentiate various human activities [Zhang et al. 2012][Ding et al. 2015], e.g., sitting and walking. Yet, the granularity of mobility quantified in existing solutions is not adequate. For example, [Zhang et al. 2012][Wang et al. 2016] can only distinguish static and mobile objects , while [Ding et al. 2015][Wang et al. 2015] deal with targets moving at similar speed. Therefore, quantifying the intensity of mobility that is closely related to typical indoor activities is not well addressed yet. One may think of making use of the

[1] IKEA Canada Engages Customers With RFID at Pop-up Store. HTTP://www.rfidjournal.com/articles/view?14719

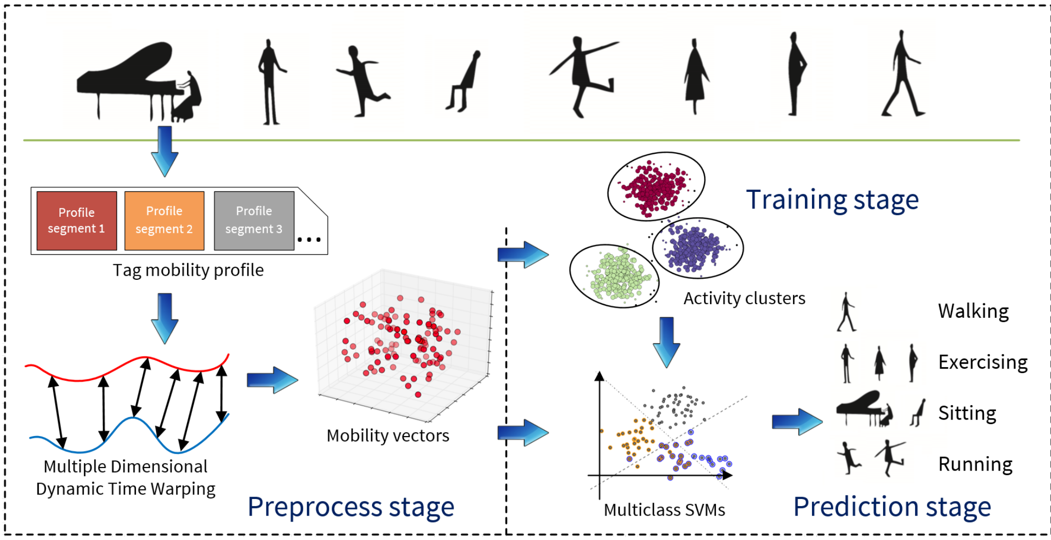

Fig. 1: Our supervised learning framework for mobility detection and activity identification

RFID localization techniques that have successfully achieved centimeter or even millimeter accuracy for mobility detection. Unfortunately, while such advanced solutions as RF-IDraw [Wang et al. 2015] and Tagoram [Yang et al. 2014] achieve high accuracy through exploring antenna arrays, their performance degrades heavily for indoor environments with multipath. Intuitively, their phase measurement, a core operation, can be remarkably affected by multipath, invalidating the key assumption [Ryoo and Das 2015] that the Angle-of-Arrival of the direct path is related to the measurement phase difference between antennas, especially in Non-Line-of-Sight (NLoS) cases. Other localization solutions relying on predeployed reference tags [Wang and Katabi 2013][Shangguan et al. 2015] generally require the tagged objects to be static or with limited the moving velocities (i.e., 0.17-0.3 m/s), which is not even applicable for walking (1$\sim$1.4 m/s) and running (5$\sim$7 m/s). Mobility may also be estimated through the doppler effect [Ding et al. 2015]. Yet it works with only static communication environments and will again become unstable in fast-changing indoor environments with dynamic multipath, random signal/thermal noise, and varying antenna orientations. Empirically, we show that prior schemes suffer from serious performance degradation for detecting realworld moving tags in typical indoor environments, since using a single parameter for mobility detection is ineffective in multipath scenarios. Our observations motivate us to adopt a profile-based mobility detection that utilizes multiple parameters in tag readings, which is detailed in Section 2.

In this paper, we present i^{2}tag, a mobility-aware activity identification system for RFID tags through intelligent profiling, which works robustly in multipath-rich indoor environments. i^{2}tag constantly generalizes a huge amount of fine-grained mobility, which further enables us to utilize a supervised learning framework for activity identification as shown in Fig. 1. At a high level, it goes through the following major steps:

— **Preprocessing stage.** we employ a novel fine-grained *mobility profile* to quantify different levels of mobility, which seamlessly integrates RSSI variance and packet loss rate, as well as a relative-phase-based fingerprint. The latter is highly effective in distinguishing tag mobility in complicated indoor environments with random signal noise and multipath. By comparing the measured mobility profile against known reference mobility profiles, we detect the tag velocity through a Multiple Dimensional Dynamic Time Warping (MDDTW) [Salvador and Chan 2007] algorithm. We classify tag mobility into multiple categories based on the estimated velocity; for instance, *stationary*, *micro-mobility*, and *macro-mobility*.[2] In this stage, we split tag mobility profile $\mathcal{P}_i = \{p_i^1, p_i^2, ...\}$ into segments in equal window size τ as $\{\mathbf{p}_i^1, \mathbf{p}_i^2, ...\}$, which will be transferred into a mobility vector as $\mathbf{v}_i = \{\nu_i^1, \nu_i^2, ...\}$, where mobility vector as an underpinning unit is applied in a multiclass support vector machine (SVM) [Knerr et al. 1990].

— **Training stage.** Each tag mobility profile $\mathcal{P}_i$ is represented by a corresponding mobility vector $\mathbf{v}_i$, then we can distinguish different kinds of activities, e.g., sitting, exercising, walking, and running. To be specific, V_{train} in training samples with corresponding labels will be trained to build the mapping σ from the feature $\mathbf{x}_i$ of mobility vector $\mathbf{v}_i$ to activity label y_i.

— **Prediction stage.** We perform activity recognition in a supervised learning way. For each mobility vector $\mathbf{v}_i \in V_{test}$, we determine whether the feature $\mathbf{x}_i$ of mobility vector is concentrated in certain activities, then label it via σ to achieve corresponding y_i.

$\mathtt{i}^2\mathtt{tag}$ is readily deployable using off-the-shelf RFID readers[3] (a single UHF reader with a limited number of antennas) and allows reusing existing RFID readers for indoor activity identification. We have implemented a prototype of $\mathtt{i}^2\mathtt{tag}$ using a `Thingmagic` reader and `Impinj` tags, and have conduct extensive experiments in indoor environments. The results demonstrate that, with $\mathtt{i}^2\mathtt{tag}$, a single RFID reader with two connected antennas can accurately distinguish the tag velocity, classify the fine-grained mobility and four categories of activities, with an average detection rate up to 96%.

The rest of the paper is organized as follows. Section 2 illustrates the motivation of our work. Section 3 provides our detailed observations on the moving tags properties, then presents activity identification to efficiently solve the problem. Section 4 shows the details of implementations. Section 5 discusses the performance evaluation results on our approach. We provide a literature review in Section 6 and we conclude this paper in Section 7.

2. WHY SINGLE PARAMETER DOESN'T WORK

2.1. Phase difference as a single value

The limited programming interface posed by commercial tag readers[4] provides only RSSI and phase values. Yet RSSIs are not reliable for location inference, especially for indoor environments, where multipath effects are dominant [Griffin and Durgin 2009]. On the other hand, the phase value is a relatively reliable choice for deriving statues of location and mobility. Intuitively, accurate RFID localization can realize tag mobility detection. The tag mobility can be distinguished by the angular velocity, depending on the spatial angle θ as well as the phase difference $\Delta\phi$ [Ding et al. 2015; Wang et al. 2015; Hekimian-Williams et al. 2010], as shown in Fig. 2(a). In this figure, one can calculate the spatial angle θ by comparing the phases of the received signals at multiple antennas. The phase ϕ of an RF signal rotates by 2π for every λ (wavelength) distance the signal travels. Let $d_{s,i}$ and $d_{s,j}$ denote the distances from the source s, to

[2]Zhou *et al.* [Zhou 2016] proposed a random mobility model for the different mobile situations, e.g., the user may slowly move the tag although he/she is stationary or his/her movement is confined within a small area.
[3]It is worth noting that the limited programming interface posed by commercial tag readers provides only RSSI and phase values. As such, advanced algorithms for powerful wireless devices are not necessarily applicable here.
[4]ThingMagic M6e RFID reader module. http://www.thingmagic.com/embedded-rfid-readers

the two antennas respectively, and ϕ_i and ϕ_j are the phases of the received signal that we measure at the two antennas. The phase difference between the received signals at the two antennas, $\Delta\phi_{j,i} = \phi_j - \phi_i$, relates to the difference in their distances from the source, $\Delta d_{j,i} = d_{s,j} - d_{s,i}$, as follows:

$$\frac{\Delta d_{j,i}}{\lambda} = \frac{\Delta\phi_{j,i}}{2\pi} + k \tag{1}$$

where k can be any integer in $[-\frac{D}{\lambda} - \frac{\Delta\phi_{j,i}}{2\pi}, \frac{D}{\lambda} - \frac{\Delta\phi_{j,i}}{2\pi}]$ and D is the distance between two antennas as Fig. 2 shows.

However, we find that the above intuition is true only when the multipath effect is negligible. As seen from Fig. 2(b), if the signal arrives each antenna via two paths, the overall phases received at the two antennas become ϕ'_i and ϕ'_j. Let s_i and s_j denote the signals along direct path from source s to antenna i and j. In Fig. 2 (b), s'_i and s'_j denote the signals along second path from source s to antenna i and j. Let α denote the amplitude of s . Let α_i, α_j,α'_i and α'_j represent the propagation attenuation at the path $d_{s,i}$, $d_{s,j}$, $d'_{s,i}$ and $d'_{s,j}$. We assume the source s is far from antennas, therefore $d_{s,i} = d_{s,j} = d$.

$$s_i = \alpha \cdot \alpha_i \cdot e^{j(\phi_0 + \frac{d}{\lambda}\cdot 2\pi)} \tag{2}$$

$$s_j = \alpha \cdot \alpha_j \cdot e^{j(\phi_0 + (\frac{d}{\lambda} + \frac{Dcos\theta}{\lambda})\cdot 2\pi)} \tag{3}$$

where $\phi_i = \phi_0 + \frac{d}{\lambda} \cdot 2\pi$ and $\phi_j = \phi_0 + (\frac{d}{\lambda} + \frac{Dcos\theta}{\lambda}) \cdot 2\pi$.

$$s'_i = \alpha \cdot \alpha_i \cdot e^{j(\phi_0 + \frac{d}{\lambda}\cdot 2\pi)} + \alpha \cdot \alpha'_i \cdot e^{j(\phi_0 + \frac{d'_{s,i}}{\lambda}\cdot 2\pi)} \tag{4}$$

$$s'_j = \alpha \cdot \alpha_j \cdot e^{j(\phi_0 + (\frac{d}{\lambda} + \frac{Dcos\theta}{\lambda})\cdot 2\pi)} + \alpha \cdot \alpha'_i \cdot e^{j(\phi_0 + (\frac{d'_{s,j}}{\lambda} + \frac{Dcos\theta}{\lambda})\cdot 2\pi)} \tag{5}$$

where $\phi'_i = 2 \cdot \phi_0 + \frac{d}{\lambda} + \frac{d'_{s,i}}{\lambda}$ and $\phi'_j = 2 \cdot \phi_0 + \frac{d}{\lambda} + \frac{d'_{s,j}}{\lambda} + 2 \cdot \frac{Dcos\theta}{\lambda}$. For instance, we assume $\phi_0 = 0$, $\lambda = 0.33m$, $\alpha = 1$, $\alpha'_i = 0.6$, $\alpha'_j = 0.7$, $\alpha_i = 0.8$, $\alpha_j = 0.9$, $\theta = \frac{\pi}{4}$,$d = 3.3m$, $d'_{s,i} = 3.5m$,$D = 0.165m$ and $d'_{s,j} = 4m$. Then $s'_i = 0.33 - 0.37i = 0.496e^{-0.8425j}$ and $s'_j = 0.1325 + 0.5404i = 0.5564e^{1.3304j}$, hence $\phi'_i = -0.8425$ and $\phi'_j = 1.3304$. Since $\phi_i = 0$ and $\phi_j = 2.2217$, we have $\phi_i \neq \phi'_i$ and $\phi_j \neq \phi'_j$. Obviously, the new phase difference under this simple multipath scenario is not equal (nor a good approximation) to the original phase difference, i.e., $\Delta\phi_{j,i} \neq \Delta\phi'_{j,i}$. Hence, these approaches are ineffective in multipath-rich indoor environments.

To verify the above hypothesis, we conduct a series of indoor experiments using off-the-shelf tags and the reader by varying positions (spatial angle θ), distances, and tag orientations. The frequency hopping affects phase-angle measurements even for a stationary tag, and thus we fix the channel on the 910 MHz. The results are plotted in Fig. 3 (a)-(c), which show that the measured phase differences are unreliable, even there exist some experimental results matched with the theoretical benchmark. (i). In Fig. 3 (a), the red dashed line is the numerical benchmark and the purple dots represent the measured phase difference values $\Delta\phi$ in the experiments. We place the stationary tag at a distance 2m facing to the polarized antennas at different spatial angle θ. it shows the phase differences are not acceptable. We observe that there are significant offsets between the measured phase difference values and the theoretical benchmark; (ii). In Fig. 3 (b), we put the tag with spatial angle $\theta = 90°$ at different distances. The result demonstrates that the distances have no influences on the phase errors, where the significant phase errors exist at any distances; (iii). In Fig. 3 (c), the

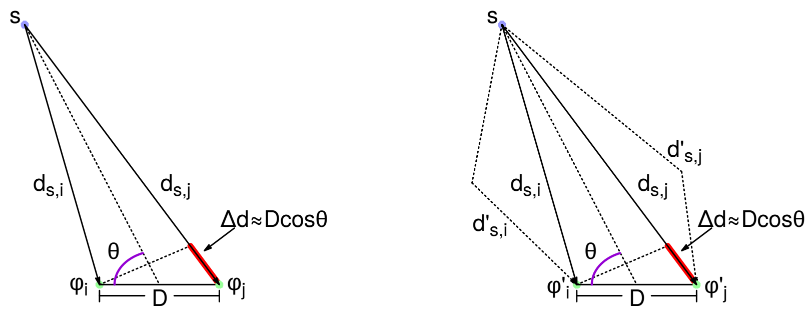

(a) Single path (b) Multiple path

Fig. 2: **Angle of Arrival at Antenna Pair:** Based on the signal phase difference measured between a pair of antennas, ideally we can estimate the spatial direction along which the source's signal arrives. Yet the phase-based approach suffers from multipath effects, where $\Delta\phi'_{j,i}$ is not reliable with $\phi'_i \neq \phi_i$ and $\phi'_j \neq \phi_j$.

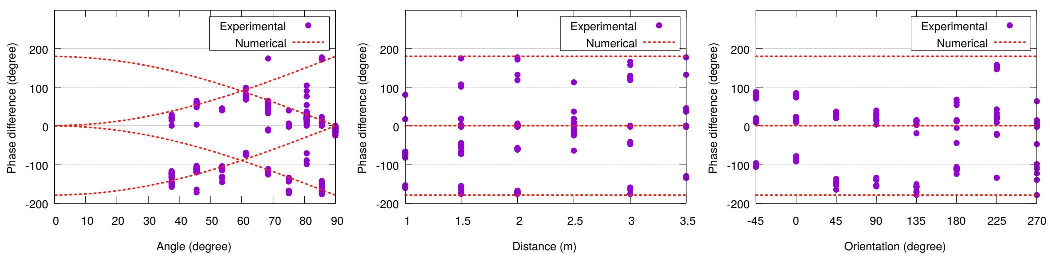

(a) Spatial angle θ, distance $d = 2m$ (b) Tag orientation, spatial angle $\theta = 90°$, distance $d = 2m$ (c) Tag orientation, spatial angle $\theta = 90°$, distance $d = 2m$

Fig. 3: Empirical results of existing methods that use the phase difference as a single value

tag orientation is defined as the angle between the reader antenna's polarization direction and the tag's antenna. It shows that the tag orientation also introduces the phase errors. Therefore, these measured phase errors as well as random signal noises exist anytime, making phased-based localization ineffective and unreliable. Even worse, a stationary RFID tag can be confused with a tag moving at a high velocity.

2.2. Phase differences as a vector

From the above, we know that the phase difference $\Delta\phi_{j,i}$ as the single parameter is ineffective in multipath scenarios. We observe that if we stack the phase differences across a small time interval into a vector, then this vector can be a good indicator of different mobility. To see how this works, we first broadly classify tag mobility into three categories. If the tag is static, it is in the *stationary* status, as Fig. 4 (a) shows. For the mobile situation, the user may slowly move the tag although he/she is stationary or his/her movement is confined within a small area, e.g., the user may make a telephone call, and a little movement of her head may displace her smartphone. We call that the tag is under *micro-mobility* in Fig. 4 (b) if it is moving but its location is confined within a small area. Otherwise, tag mobility may also cause the tag to change its location as

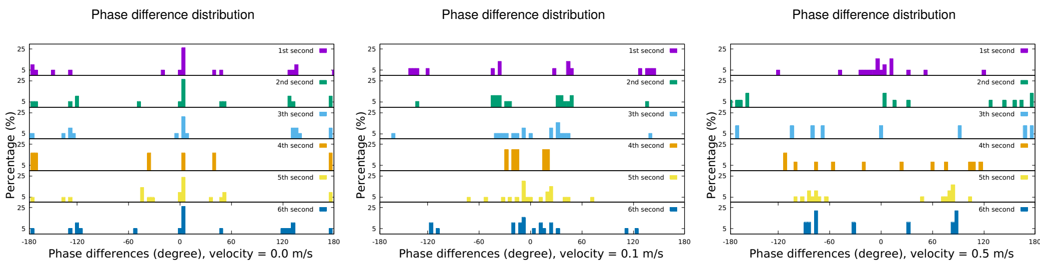

(a) Stationary tag (b) Micro-mobility tag (c) Macro-mobility tag

Fig. 4: Our observation that the phase difference vector can be a good indicator for different levels of mobility.

its user walks from one location to another. In such scenarios as Fig. 4 (c), we classify the tag to be under *macro-mobility*.

We run three experiments to analyze each kind of mobility in multipath environments. First, we place a stationary tag at a fixed location. Second, for micro-mobility tag, we picked up the tag and moved it around within a meter of its location. Lastly, for evaluating macro-mobility tag, we walked around with the tag in our hand. Fig. 4 (a) depicts the phase difference for the three categories of tags in 6 seconds. In Fig. 4 (a), the reader received the signals from a stationary tag, where the phase difference distribution keeps relatively stable. Both the micro-mobility tag with velocity 0.1 m/s in Fig. 4 (b) and macro-mobility tag with velocity 0.5 m/s in Fig. 4 (c) return the phase values, where we clearly see that the variance of the phase differences from the macro-mobility tag increases much faster than those of the micro-mobility tag.

We shall explore more details of the relative phase fingerprint in the next section. To detect the tag mobility, we propose a concept of *relative phase fingerprint*, which denotes the Bhattacharyya distance [Djouadi et al. 1990] of the phase difference distribution between two intervals. For illustration, we extract the phase difference distribution at 5 s and 6 s; as can be seen, the stationary tag has much more similarity of phase difference distribution between the two seconds.

3. SYSTEM DESIGN

This section starts from the design of our mobility profile. Then we have shown how to use this profile to effectively detect mobility. Finally, we showcase an accurate indoor activity identification system that builds on our mobility detection scheme.

3.1. Mobility Profile

Before we proceed with the detailed solutions for the individual modules of $\mathtt{i}^2\mathtt{tag}$, we first summarize the key notations in Tab. I. The read operation of a commercial UHF RFID reader contains the metadata, namely *measured mobility profile*, about how, where and when the tag was read. The measured mobility profile for each tag read is as follows: antenna ID, read count, timestamp, frequency, phase, and RSSI. We utilize the RSSI, phase and read count for detecting tag mobility.

3.1.1. RSSI. One possibility is to utilize the RSSI of the tag, although RSSI values in backscatter communication are not sensitive with the mobility of tags. To provide empirical evidence of the above claim, we measure the RSSI values on ten channels from 910-915 MHz. In our experiments, we found that RSSI is quite stable in stationary scenarios. Yet RSSI is susceptible to any changes in the environment. Often, the RSSI

t_i	time i
τ	window size
T	number of periods
$\Delta\phi_i^{t_j}$	phase difference for tag i at time t_j
ψ_i	phase difference density at time i
φ_i	phase difference histogram at time i
r_i^j	RSSI variance of tag i at time j
s_i^j	relative phased-based fingerprint of tag i at time j
e_i^j	packet loss rate during of tag i at time j
p_i^j	measured mobility profile of tag i at time j
$\mathbf{p}_i^k$	mobility profile segment of tag i
$\mathcal{P}_i$	mobility profile for tag i
$\mathbb{P}$	a set of tag profile $\{\mathcal{P}_1, \mathcal{P}_2, ...\}$
$\mathcal{D}$	distance matrix
$\mathcal{L}$	warping path
$C_{\mathcal{L}}$	total cost of warping path
$\mathbf{v}_i$	mobility vector for tag i
ν_i^j	mobility status
$\mathbf{f}_i$	mobility feature
y_i	activity label
c_i	activity cluster

Table I: Summary of Notations

variance under environmental mobility is higher than the observed variation in device mobility.

Fig. 5(a) shows the velocity and corresponding RSSI when the tag is stationary or of other mobility. When the tag is close to the RFID reader, RSSI values are naturally high; yet there are few differences between the stationary tag and moving tags. Therefore, RSSI values cannot be immediately applied in the mobility detection. Fortunately, we observe that the significant differences in RSSI variance between the stationary and moving tags, where we normalize the RSSI variance value between 0 and 1. Although there are multipath in the indoor environment, the RSSI variances of static tags keep relatively stable. There is a significant difference between stationary and moving tags, where the RSSI variances change frequently due to the changing tag position and multipath. Fig. 5(b) shows the RSSI variance at the different tag velocity, where we use normalized standard deviation to represent the RSSI variance, which is range from 0 to 1. Clearly, the RSSI variance can be used to distinguish between stationary and mobility scenarios, where the RSSI variance of velocity 0 m/sec is close to 0.21 and the RSSI variance of velocity 0.2 m/sec jumps to 0.35. The error bars are high for the moving tags; therefore it is difficult to distinguish between micro-mobility and macro-mobility using the RSSI variance.

3.1.2. Packet Loss Rate. Packet loss rate, another important metric in backscatter systems, is the percentage of the maximum number of times that the tag was read during a fixed interval, e.g., one second. Intuitively, mobility and packet loss rate are strongly correlated, since mobility often leads to fast-changing channels.

Hence, the measured packet loss rate can be a dependable indicator of dynamic channel quality. Intuitively, we can use the difference in the loss rates to infer how the tag changes in location or mobility velocities. The experimental results support this hypothesis as shown in Fig. 5(b), which clearly shows that it is straightforward to distinguish between the mobile and stationary case since they have the vastly different packet loss rates. Thus, the packet loss rate is a unique feature of backscatter commu-

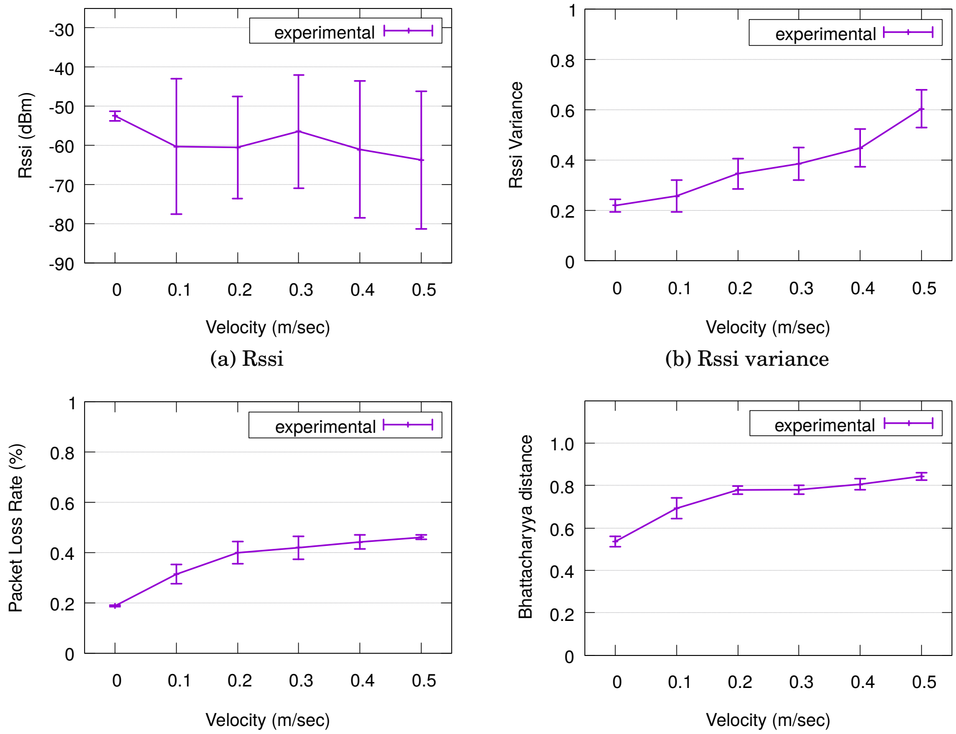

(a) Rssi (b) Rssi variance (c) Packet loss rate (d) Relative phase fingerprint

Fig. 5: Multi-dimensional mobility profile

nication, which involves complementary information about path loss and multipath effects. However, there are still large overlaps between different classes of mobility. Since the loss rate is measured from each of received packets, the moving operation makes the packet loss rate of RFID tag increases rapidly. As such, even if it is possible to use loss rate to distinguish between stationary and macro-mobility, it cannot reliably distinguish between different classes of device mobility.

3.1.3. Relative phase fingerprint. We have demonstrated that the measured phase cannot be applied to mobility detection in multipath-free environments. Here, we propose a concept of *relative phase fingerprint* to represent the similarity of phase difference distributions.

Instead of directly using the phase differences, we use histogram formulation to represent the distribution of phase differences at a short interval. The reader antennas receive a set of consecutive signals from the moving tag, where we can capture a set of phase differences $\psi_i = \{\Delta\phi_i^{t_j}, \Delta\phi_i^{t_{j+1}}, ...\}$ between two antennas. Let ψ_i be the phase difference density of the moving tag, which is discretized into m-bins with the function $\varphi_i = h(\psi_i)$. The histogram φ_i is produced by assigning phase differences $\psi_i = \{\Delta\phi_i^{t_j}, \Delta\phi_i^{t_{j+1}}, ...\}$ to the corresponding bin.

The estimated state of tag mobility is updated at each time step by incorporating the new observations. Our measurement of the distance between the two phase distributions φ_i and φ_j is based on the Bhattacharyya coefficient [Djouadi et al. 1990]. Considering discrete densities such as our phase difference histograms $\varphi_i = \{\varphi_i^1, \varphi_i^2, ..., \varphi_i^m\}$ and $\varphi_j = \{\varphi_j^1, \varphi_j^2, ..., \varphi_j^m\}$, the coefficient is defined as

$$\rho(\varphi_i, \varphi_j) = \sum_{u=1}^{m} \sqrt{\varphi_i^u \varphi_j^u} \tag{6}$$

where m is the number of bins. The larger ρ is, the more similar the distributions are. For two identical normalized histograms we obtain $\rho = 1$, indicating a perfect match. We define the distance between two distributions as

$$d = \sqrt{1 - \rho(\varphi_i, \varphi_j)} \tag{7}$$

where d is also called the Bhattacharyya distance [Djouadi et al. 1990]. We use this d to quantify the similarity of relative phase fingerprints.

Fig. 5(c) illustrates that the Bhattacharyya distance of the relative phase-based fingerprint can be used to detect the tag velocity. For slow velocity, the Bhattacharyya distance stays low due to the stable environment and slow changes of the phase differences. The Bhattacharyya distance increases once the tag keeps moving. Furthermore, we found that the similarity of fast moving tag (0.4-0.5 m/s) increases faster than slowly moving tag (0.2-0.3 m/s). This happens because a slowly moving tag typically affects only a few multipath components, whereas if the tag itself is moving, all the multipath components will be affected. Therefore, the RFID signal experiences faster variation under macro-mobility than under micro-mobility for the relative phase-based fingerprint.

3.2. Mobility Detection

In this section, we introduce an approach to determine mobility statuses of tags. The mobility profile is constantly changing over time with the tag rotation and change of locations. Note that the mobility profile patterns are similar for the same mobility at different rounds but distinctive for different mobility. That said, a particular mobility can be identified by comparing against known profiles.

During the period T of interval length τ, we have the mobility profile set $\mathcal{P}_i$ of RFID tag i with RSSI variance $R_i = \{r_i^1, r_i^2, ..., r_i^T\}$, relative phase-based fingerprint $S_i = \{s_i^1, s_i^2, ..., s_i^T\}$ and the packet loss rates $E = \{e_i^1, e_i^2, ..., e_i^T\}$. We have mobility profile $p_i = \{r_i, s_i, l_i\}$ in interval t_i and mobility profile $\mathcal{P}_i$ as follows:

$$\mathcal{P}_i = \{\underbrace{p_i^1, p_i^2, ..., p_i^\tau}_{1st\ seg}, \underbrace{p_i^{\tau+1}, ..., p_i^{2\tau}}_{2nd\ seg}, ..., \underbrace{p_i^{(k-1)\tau+1}, ..., p_i^{k\tau}}_{kth\ seg}, ...\} \tag{8}$$

where τ is the windows size of segments. Let mobility profile segment $\mathbf{p_i}^k$ represent the k_{th} segment in the mobility profile $\mathcal{P}_i$.

$\mathtt{i^2tag}$ detects the tag mobility based on the distance with the multiple dimensional vectors, i.e., the RSSI variance, packet loss rates and relative phase-based fingerprint. To perform multidimensional sequence alignment, $\mathtt{i^2tag}$ employs Multi-Dimensional Dynamic Time Warping [Salvador and Chan 2007] to compute the similarity between two mobility profiles. On one hand, MDDTW compares two mobility profiles with different lengths. On the other hand, MDDTW automatically compresses or stretches a sequence to minimize the distance between two sequences, thus focusing on the shape similarity rather than the absolute values.

We capture the mobility profile based on the tag velocity as the reference $\mathbb{P} = \{\mathcal{P}_1, \mathcal{P}_2, ...\}$. Then we use the Multiple Dimensional Dynamic Time Warping (MDDTW) technique to match the reference mobility profile against the measured mobility profile. It naturally compensates for the shifts among different mobility profiles caused by varying tag moving velocities. The input of the MDDTW algorithm consists of a reference mobility profile $\mathcal{P}_i$ of length N and a measured mobility profile $\mathcal{P'}_j$ of length M. MDDTW first constructs a distance matrix $\mathcal{D}_{M\times N}$ where each element D_{uv} is defined as the Euclidean distance between element p_i^u and p_j^v:

$$\mathcal{D}_{uv} = p_i^u - {p'}_j^v = ||r_i^u - {r'}_j^v|| + ||s_i^u - {s'}_j^v|| + ||e_i^u - {e'}_j^v|| \tag{9}$$

where p_i^u and ${p'}_j^v$ are the u_{th} and v_{th} elements of the mobility profiles $\mathcal{P}_i$ and $\mathcal{P'}_j$, respectively. The MDDTW algorithm find a warping path $\mathcal{L}(\mathcal{P}_i, \mathcal{P'}_j) = \{l_1, l_2, .., l_k\}$ such that the total cost $C_L(\mathcal{P}_i, \mathcal{P'}_j)$ of the warping path is minimized:

$$\arg\min_{\mathcal{L}} C_{\mathcal{L}}(\mathcal{P}_i, \mathcal{P'}_j) = \sum_{i=1}^{k} \mathcal{D}_{l_i} \tag{10}$$

where $l_i = (x, y) \in [1 : M] \times [1 : N]$. Then the measured mobility profile $\mathcal{P'}_i$ is classified into different mobility based on the reference mobility profile set $\mathbb{P}$. Algorithm. 1 shows the workflow to calculate the mobility vector $\mathbf{v}_i = \{\nu_i^1, \nu_i^2, ...\}$ for each RFID tag mobility profile $\mathcal{P'}_i$, which contains a sequence of mobility status.

ALGORITHM 1: Mobility detection

```
Input: reference mobility profile set ℙ, and measured mobility profile set ℙ'
Output: a set of mobility vector {v_i}
for each P'_i ∈ ℙ' do
    Mobility vector v_i = ∅;
    j = 0;
    ν_i^j = 0;
    for each p'_i^j ∈ P'_i do
        Cost = +∞;
        for each P_k ∈ ℙ do
            C_tmp = C_L(p'_i^j, P_k);
            if C_tmp < Cost then
                Cost = C_tmp;
                ν_i^j = k;
            end
        end
        j += 1;
    end
    mobility vector v_i = {v_i, ν_i^j};
end
Return a set of mobility vector {v_i};
```

3.3. Understanding the Activities

In the preprocessing stage, we first set a window size τ to split the tag mobility profile $\mathcal{P}_i$ into profile segments $\{\mathbf{p}_i^1, \mathbf{p}_i^2, ...\}$ as illustrated in Fig.1. For each profile segment $\mathbf{p}_i^j$, we treat it as the basic unit and extract its mobility status ν_i^j for labeling. In this section, we will introduce the multiclass SVMs on recognizing and labeling the activities based on the tag mobility vector $\mathbf{v}_i$. For each mobility vector $\mathbf{v}_i$, we could simply calculate mobility frequency and denote it as feature $\mathbf{f}_i$ that means the mobility percentage.

When all preparatory steps are done, we can identify the activities in mobility profile $\mathcal{P}_i$. We assume that there are multiple categories of activities in one specific mobility profile. Specifically, if we have a semantically concentrating profile, for the mobility frequencies, they may have higher variances and lower information entropy. We accordingly formulate the concentrating rating γ as follow:

$$\gamma = \frac{\sum_i^k (f_i - \bar{f})}{\sum_{\mathbf{q}} -q \log(q)} \tag{11}$$

in which $\mathbf{q}$ is the normalized form of $\mathbf{f}$, i.e., $q_i = \frac{f_i}{\sum_j f_j}(f_i \neq 0)$, and $\sum_{\mathbf{q}} -q\log(q)$ here is indeed the entropy of $\mathbf{q}$. Then, mobility profile segments $\{\mathbf{p}_j^{t_s}, ..., \mathbf{p}_j^{t_e}\}$ with their concentrating ratings larger then a threshold will be recognized as an activity segment $\mathbf{x}_i =< t_s, t_e, \mathbf{f}_i >$, where t_s,t_e indicates the time range of slide, $\mathbf{f}_i$ means the comment frequency on the mobility.

Note that the threshold here is set dynamically in different mobility profiles. We can calculate a series of ratings for the slides and then find the max and min. The threshold is set as $\alpha \times min + (1-\alpha) \times max, (0 \leq \alpha \leq 1)$, where α is called pass rate and the sensitiveness of α will also be discussed in experimental part.

The set of activity segment $\mathbf{x}_i =< t_s, t_e, \mathbf{f}_i >$ are now obtained, and we label each feature $\mathbf{x}_i$ with our preset activity label y_i in a supervised way. We investigate the use of kernel functions to transform the mobility space into a feature space amenable to the Support Vector Machine (SVM) learning methods [Knerr et al. 1990]. SVMs work well in many learning situations since they generalize to unseen data, where the machine is defined by a subset of the training points (i.e., support vectors). In the basic binary classification, SVMs find a hyperplane that provides a maximal separation between two classes. This optimal hyperplane is orthogonal to the shortest line connecting the two classes in their dimensional space, where SVMs maximize the minimal margin. Additional data points, i.e., noises, do not affect the final solution unless they redefine the margin. Therefore, SVMs are amenable to continuous, adaptive on-line learning in activity identification. Multiclass SVMs [Knerr et al. 1990] solves the problem of classifying instances into the more than two classes.

We start with the supervised case. Assume we are given labeled training examples $(\mathbf{x}_1, y_1), ..., (\mathbf{x}_n, y_n)$, where each example is assigned a label from a fixed finite set $y_i \in \{1, ..., k\}$, where k is the total number of categories of activities. Here, we need to extend our feature functions $\sigma(\mathbf{x}, y)$ to include the y-labels explicitly, which provides a separate weight vector $\mathbf{w}_k$ for each class k. Once a complete weight vector has been learned, subsequent test examples $\mathbf{x}$ are classified according to $y^* = \arg\max_y \mathbf{w}^\top \sigma(\mathbf{x}, y)$. The dominant multi-class training procedure for SVMs is formulated as:

$$\begin{gathered} w = \min_{\mathbf{w},\boldsymbol{\xi}} \frac{\beta}{2}||\mathbf{w}||^2 + \boldsymbol{\xi}^\top \mathbf{e} \\ s.t.\ \ \mathbf{w}^\top(\sigma(\mathbf{x}_i, y_i) - \sigma(\mathbf{x}_i, k)) \geq \delta(y^i, k) - \xi_i, \forall_{i,k} \end{gathered} \tag{12}$$

where $\delta(y_i, k) = 1_{(y_i \neq k)}$, and w is the multi-class analog of the inverse squared margin. When we get the classifier, every activity segment $\mathbf{x}_i$ can be labeled with a human understandable activity lable y_i. In our case, multiclass SVMs [Knerr et al. 1990] are chosen to perform robust and efficient multi-classfication.

(a) ThingMagic M6e RFID reader

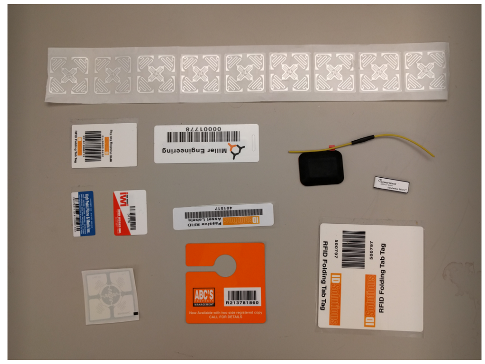

(b) Various RFID tags

(c) Laird Indoor RFID antennas

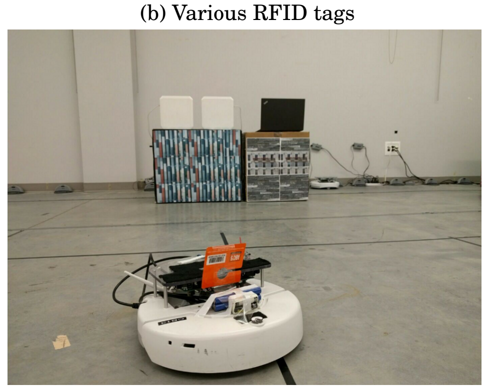

(d) iRobot Create Programmable Robot

Fig. 6: Commercial UHF RFID devices used in experiments

4. IMPLEMENTATION

In this section, we describe the key implementation details that are not covered in the previous sections. Our implementation is entirely done based on a commercial reader and requires no modifications to tags. Note that we only highlight the key components here since any real-world activity recognition system requires enormous efforts on implementations [Aggarwal and Ryoo 2011].

Hardware settings: Although our system design works with most of the off-the-shelf commercial readers, our prototype implementation uses a Thingmagic reader over other readers (e.g., ImpinJ reader), which have been extensively used in the previous research [Wang and Katabi 2013][Shangguan et al. 2015][Ding et al. 2015]. The Thingmagic reader works well for mobile applications. For example, the dimensions of a Thingmagic Nano-RFID reader module are 22 $\times$ 26 $\times$ 3.0 mm [5], whereas those of an ImpinJ reader R420 are 190.5 $\times$ 175.3 $\times$ 30.5 mm. Additionally, the ImpinJ reader can report phase readings ranging from to $0°$ to $360°$. In contrast, our ThingMagic M6e 4-port UHF RFID reader(69 $\times$ 43 $\times$ 7.5 mm) shown in Fig. 6(a), is only able to return phases ranging from $0°$ to $180°$, which causes ambiguity. Fortunately, our system design does not require accurate phase difference measurement which is necessary for existing methods [Wang and Katabi 2013][Shangguan et al. 2015]. As $\texttt{i}^2\texttt{tag}$ relies on relative phase differences, such ambiguity poses negligible influence.

[5]Note that the ThingMagic (http://www.thingmagic.com) offers the smallest embedded UHF RFID reader modules.

Another important setting is the distance of two antennas. We connect our ThingMagic M6e reader to the two Laird Indoor RFID Antennas[6], of which the dimensions are $259 \times 259 \times 33$ mm. Theoretically, the antenna separation D should be spaced by λ/2, which effectively reduces the ambiguity caused by the high-resolution grating lobes [Wang et al. 2015]. Due to the available frequencies of RFID, the typical wavelength λ is 0.32786 m (suppose $f = 915$ MHz). Therefore, it is impossible to set D to be smaller than $\lambda/2$ (i.e., 0.16 m). In our implementation, we set D as multiples of $\lambda/2$, $D = 2 \cdot \lambda/2$, which equals to 0.33 m. Although this setting unavoidably introduces ambiguity in phase measurement, unlike RF-IDraw [Wang et al. 2015] that employs multiple antennas (8) to eliminate this ambiguity, we solve this problem using relative phase differences with only two antennas.

We examine various UHF RFID tags as shown in Fig. 6(b), where those different tags have similar performance with phase differences up to 5°. Therefore, we only report the results of a representative type, i.e., Impinj UHF RFID tags, in the rest of this paper. In our lab, we run the client on a Lenovo laptop (ThinkPad T560), equipped with an Intel Core i5-6200U Dual 2.3/2.8GHz CPU and 8 GB 1333 MHz DDR3 RAM. The server runs on a state-of-the-art Dell desktop (OPTIPLEX 7010), each equipped with an Intel Core i7-3770 3.4 GHz quad-core CPU, 8 GB 1333 MHz DDR3 RAM, and a 1 Gbits/sec Network Interface Card (NIC).

Software settings: The system employs a typical client-server architecture. The processes on clients adopt LLRP protocol [Protocol 2007] to communicate with the reader, and continuously collect the tag readings. The backend module of $\texttt{i}^2\texttt{tag}$ on the server allows mobile clients to submit the streaming of tag readings, where we store the training results in the MySQL database and execute our algorithms to detect the tag mobility and identify the activity. The Multi-Dimensional Dynamic Time Warping is implemented by C++ language and the multiclass SVMs are implemented based on the Scikit-learn library [Pedregosa et al. 2011] and LIBSVM [Chang and Lin 2011]. The client is implemented using Java and Mercury API[7]. $\texttt{i}^2\texttt{tag}$ requires the reader continuously collect tag readings for the further analysis, while using a loop to execute the tag reading operation in a duration leads an excessive delay. Therefore, we utilize the asynchronous reading method *startReading()*, which returns immediately a sequence of RFID reads to the calling thread, then the calling thread uploads the tag readings to the server.

Mobility and activity detection: Our experiments include two parts: the mobility detection and activity identification. In the mobility detection, the ground-truth of RFID tag velocity is important for the quality of training set in mobility detection, which also incurs high overhead. Then we employ a carrier attached an Impinj UHF RFID tag as shown in Fig. 6(d). The carrier is an iRobot Create programmable robot[8], of which we can accurately control moving directions and velocities. The robot runs with two powered wheels, while a third passive caster wheel maintains balance. The wheels are controlled independently with a maximum velocity of 500 mm/s. We program the iRobot moving back and forth along a line at a constant velocity. Alternatively, the robot may move along a circle, yet the velocity is uncontrollable and difficult to measure. We examine the effectiveness of tag mobility detection with different forwarding velocities ranging 0.0 m/s to 0.5 m/s. If the velocity is smaller than 0.1 m/s, the tag would be deemed *stationary*. For velocities ranging from 0.1 m/s to 0.4 m/s, we classify them as *micro-mobility*, whereas velocities that are greater than 0.4 m/s are deemed as *macro-mobility*.

[6]Laird S9028PCR/S8658PCR (RHCP) INDOOR RFID ANTENNA. HTTP://rfid.atlasrfidstore.com/
[7]Mercury API Programmer's Guide. www.thingmagic.com/
[8]iRobot Create Open Interface (OI) Specification. HTTP://www.irobot.com/

In the activity identification, we invite ten volunteers and each volunteer [9] is attached to an Impinj UHF tag on one's hand. The volunteers stand 2-5 meters away from the reader antennas in our experiments[10]. To conduct a comprehensive evaluation, we test four typical indoor activities, i.e., sitting, exercising, walking and running. In each activity case, the RFID reader continuously queries RFID readings for ten minutes. Then we evaluate the accuracy of activity identification and further explore mobility distributions for the four categories of activities. Furthermore, the volunteers conduct several different kinds of activities in one duration. They are used to evaluate the robustness of i^{2}tag for identifying randomly changing activities.

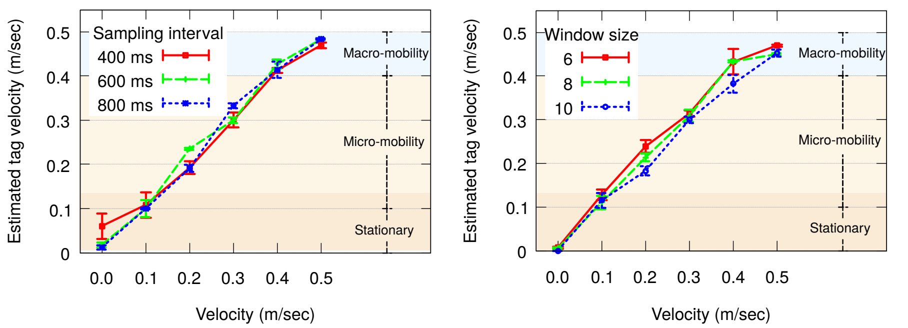

(a) Mobility detection for various sampling intervals (b) Mobility detection for various windows sizes

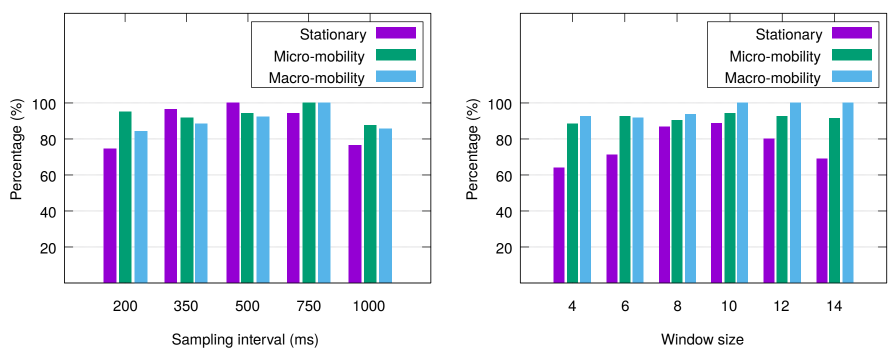

(c) Mobility detection for various sampling intervals (d) Mobility detection for various windows size

Fig. 7: Mobility detection under various conditions

5. EVALUATION

We conduct experiments in a typical office, which is a multipath-rich environment. We evaluate the performance of i^{2}tag in terms of accuracy, effectiveness, and overhead.

---

[9]Note that those volunteers are varied in age, gender, height, and weight.
[10]The commercial RFID reader's range limits the range of our current prototype. Beyond 5 meters, the RFID tag cannot harvest enough energy to wake up.

5.1. Mobility accuracy

Fig. 7 shows the result of fine-grained mobility detection accuracy with respect to carrier velocities varying from 0.0 m/s to 0.5 m/s. In particular, Fig. 7(a) plots the performance of $\mathtt{i^2tag}$ with different sample intervals. The accuracy is low for short sampling intervals, because the phase differences may not be stable even under *stationary* status. Fig. 7(b) illustrates that the larger the detection window size is, the greater the accuracy achieves. But the large detection windows size will delay the mobility detection. In this work, we identify three broad categories of tag mobility based on velocities.

Then we further evaluate the accuracy of mobility detection. The performance of detecting mobility depends on the sampling period in Fig. 7(c). The accuracy is low for short sampling period because the RFID signal of the stationary tag may change very quickly under multipath effects. We use a sampling period of 750 ms in the rest of our evaluation, yielding a median accuracy of 96%. The larger detection window size make the accuracy higher for the moving tag in Fig. 7(d). Meanwhile, large detection windows will delay the macro-mobility detection. Nonetheless, we find that a detection window of 8 yields a satisfactory accuracy of 98%, and hence we use this setting in the rest of experiments.

We next evaluate the robustness of $\mathtt{i^2tag}$ with two citations, i.e., tag orientation and distance. **Impact of orientation:** The tag orientation is defined as the angle between the reader antenna's polarization direction and the tag's antenna. To understand the effect of tag orientation, we conduct 6 experiments on the fixed frequency, 915 MHz. To measure its influence on the detection accuracy, we adjust the orientation from $0°$ to $360°$. As expected, the result remains at the same level. **Impact of distance:** We evaluate the accuracy with varying distances from 1 m to 3 m. $\mathtt{i^2tag}$ does not exhibit clear correlation with the distance. Therefore, the distance is not a crucial factor affecting the accuracy. Especially, a mean error distance of 5 mm can be obtained, when placing the antenna at a distance of 0.3 m. In fact, it is more reasonable to model the antenna as a point locating at its centroid when it keeps far away from the tag.

5.2. Activities and mobility

	Identified activities percentage (%)			
	Sitting	Exercising	Walking	Running
Sitting	94.62	5.38	0	0
Exercising	12.50	87.50	0	0
Walking	0	15.00	75.00	10.00
Running	0	0	24.44	75.56

Table II: Activity identification of single RFID tag

Tab. II shows the results of activity recognition for a single tag. Each row denotes the actual activity performed and each column represents the activity recognized by $\mathtt{i^2tag}$. Each element in the matrix represents the percentage of activities in the row, which is recognized as the activity in the column. As shown in the table, the average accuracy is 83.15% for four activities. This shows that we can extract rich information about the tag mobility and activities. The result clearly shows that $\mathtt{i^2tag}$ achieves a high and stable activity recognition performance, due to its efficient mobility detection and robust activity cluster algorithms. The average accuracy of identifying activities is 83.15%, where the slow activity identification have the accuracy up to 94.62%. The above results show that $\mathtt{i^2tag}$ can distinguish a set of activities with high accuracy.

	Identified activities percentage (%)			
	Sitting	Exercising	Walking	Running
Walking	0	0	70	30
Running	0	0	10	90
Sitting	96	4	0	0
Exercising	0	80	20	0
Exercising	10	78	12	0
Exercising	8	82	10	0
Exercising	0	85	15	0
Walking	0	0	90	10

Table III: Activity identification of two RFID tags

To understand the effect of multiple activities in one sequence of tag readings, we conduct four experiments, where there are two kinds of activities operating in order. In each experiment, an activity is performed for 5 minutes. $\mathtt{i^2tag}$ can clearly distinguish those activities based on the tag mobility distribution as shown in Tab. III. We further have a detailed look at these experiments as shown in Fig. 8. Fig. 8(a) shows that walking and running have no stationary status, where activity has approximately 90% macro-mobility and walking only has 25% macro-activity. Fig. 8(b) illustrate the high percentage of stationary and micro-mobility represents the activity is in a small area. Fig. 8(c) illustrates the same kind of activity that has the similar percentage of stationary and mobility status, where two volunteers just walked and did some daily routines. Fig. 8(d) shows that micro-mobility and macro-mobility are effective to distinguish different intensities of mobility.

5.3. Realtime performance

$\mathtt{i^2tag}$ provides online mobility-detection and activity identification, where the statistical information is displayed in Tab. IV. $\mathtt{i^2tag}$ takes an incremental process to generate the relative phase-based fingerprint. After receiving a successful response from the reader, $\mathtt{i^2tag}$ produces intermediate tag features and superimposes them to the Multiple-dimensional Dynamic Timing Warping processing. The read time is the interval during which the reader interrogates two consecutive rounds of reading. It is an upper bound which should be taken for producing an intermediate result. The median read time is 33 ms, and any computation exceeding this bound might affect the real-time performance. Theoretically, the fast implementation of Multiple Dimensional Dynamic Timing Warping (MDDTW) provides optimal or near-optimal alignments with an $O(n)$ time and memory complexity. It shows that $\mathtt{i^2tag}$ achieves a recognition latency of 30 ms on average. Therefore, we can conclude that $\mathtt{i^2tag}$ can provide real-time activity identification results.

	Window size					
Intervals (ms)	4	6	8	10	12	14
200	0.025	0.032	0.036	0.041	0.050	0.054
350	0.022	0.021	0.025	0.029	0.033	0.037
500	0.018	0.018	0.021	0.024	0.031	0.031
750	0.017	0.018	0.021	0.023	0.028	0.031
1000	0.018	0.018	0.021	0.024	0.025	0.031

Table IV: Computation Complexity

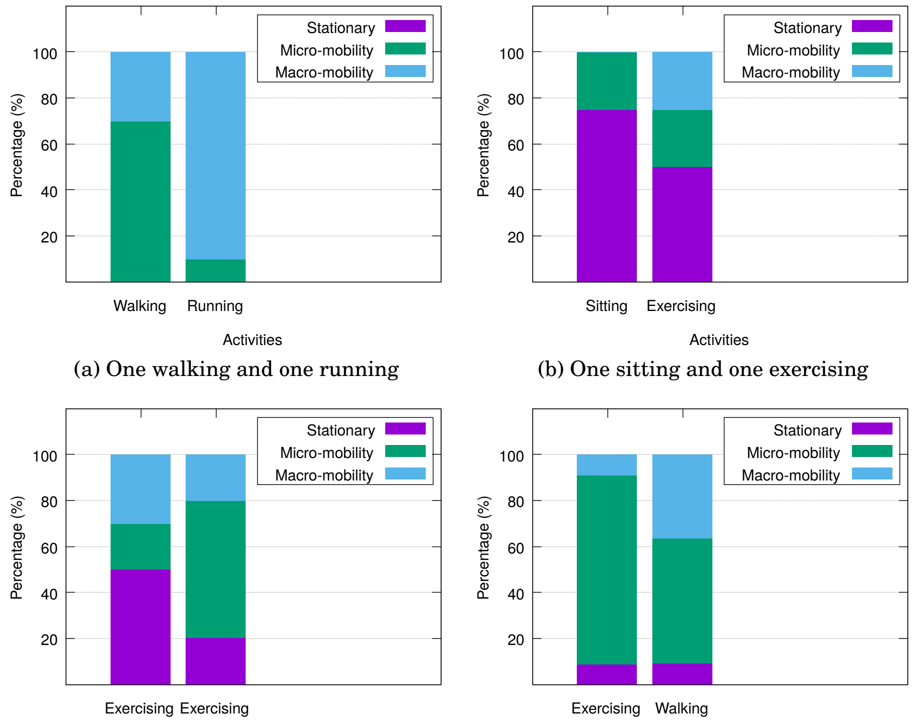

(a) One walking and one running (b) One sitting and one exercising

(c) Two exercising (d) One exercising and one walking

Fig. 8: Activities and mobility pattern

6. RELATED WORK

6.1. RSSI-based localization

Previous work on RF-based positioning primarily relied on RSSI information [Bahl and Padmanabhan 2000][Ni et al. 2004][Zhao et al. 2007][Chintalapudi et al. 2010][Rai et al. 2012]. The RF fingerprinting, pioneered by Radar [Bahl and Padmanabhan 2000], employs RSSI based fingerprinting matching against a database to determine the indoor location. LANDMARC [Ni et al. 2004] introduces the RF fingerprinting technique to RFID localization. Vire [Zhao et al. 2007] used imaginary reference tags, referred to as “virtual tags” to achieve higher accuracy. EZ [Chintalapudi et al. 2010] requires site surveys at only a few user locations. Later several other improvements over RSSI fingerprinting have been proposed, such as incorporating inertial sensor hints [Rai et al. 2012]. They typically deployed reference tags on a monitoring region and then use RSSI values to locate a specific tag. The major limitation of RSSI-based approaches is unreliable, since RSSI measured values are highly sensitive to multi-path effects, and thus difficult to achieve high-precision localization. Other works on device-free localization rely on RSSI fingerprints [Youssef et al. 2007][Seifeldin et al. 2013], which are generated in the training phase by requiring a person to stand in different locations throughout the area of interest. In the testing phase, they localize a person by mapping the resulting RSSI to the closest fingerprint

6.2. Phase-based localization

Phase reflects the distance that a wireless signal traverses in the physical world. There is growing interest in using phase measurement for localization:

6.2.1. Distance ranging. One of the simplest approaches is to calculate the distance between the transmitter and receiver based on received phase measurements. Here, we discuss only some recent and relevant works. Li *et al.* [Li et al. 2009] propose a multi-frequency based ranging method for passive RFID tag localization. Using phase measurement for distance ranging, theoretically, could achieve high localization accuracy. Due to the multipath effects, the phase measurement is not corresponding to the dominated path, and leads to high ranging error. Liu *et al.* [Liu et al. 2014] presents an RFID localization scheme by using multiple antennas to receive phase measurements from tags, where the hyperbolic positioning method is employed to correlate phase measurements.

6.2.2. Holography. Holography is the science and practice of making holograms, which is introduced to both the radar and acoustic community for target localization [Younis et al. 2003]. Miesen *et al.* [Miesen et al. 2011] employ holography to locate a moving tag on a transponder. It achieves an overall accuracy of 7 cm. Parr *et al.* [Parr et al. 2013] exploit tag mobility and adopt Inverse Synthetic Apertures Radar (ISAR) to generate hologram for tag localization and tracking. Tagoram [Yang et al. 2014] assumes that the tag movement velocity and its moving track is known in advance, and leverages the tag mobility to construct a virtual antenna array and build a differential augmented hologram using the phase values collected from the antennas. While it fails to address the multipath issue, hence will likely experience practical problems indoors where multipath reflections are prevalent and strong. $\mathtt{i^2tag}$ is inspired by above works in phase-based tag localization, but advances them by proposing a robust method based on the relative phase-based fingerprint.

6.2.3. Angle-of-Arrival(AoA). Phased-based approaches use antenna arrays or simulated multiple antennas to extract the AoA from RF signals, which can achieve a positioning accuracy on the order of tens of centimeters. Wong *et al.* [Wong et al. 2008] investigates the multiple antenna wireless local area network technologies, such as 802.11n, to perform indoor network-based positioning using angle of arrival (AOA) estimation. ArrayTrack [Xiong and Jamieson 2013] adds a novel multipath suppression algorithm to achieve sub-meter accuracy in a multipath-rich environment. SpotFi [Kotaru et al. 2015] provides accurate indoor localization services using COTS WiFi NICs with three antennas, which achieves an accuracy of 40 cm in multipath rich environments.

AoA information is also employed specifically for RFID localization. Wang *et al.* proposed PinIt [Wang and Katabi 2013], which employs a moving antenna to measure the multipath profiles of reference tags at known positions and locates the target tag. PinIt [Wang and Katabi 2013] uses synthetic aperture radar (SAR) with the moving antenna to extract the multipath profiles for each tag and leverages the reference tags to locate the target tag. PinIt is not appropriate in our mobile context because the fast-changing environment violates the tag's multipath profile at every moment, even the movement is very small. STPP [Shangguan et al. 2015] moves the mobile RFID reader with one directional antenna to acquire the spatial order of tags without localizing them. Either the tags or the mobile RIFD reader has to move at a constant velocity, while the other kind of device should keep stationary. Ryoo *et al.* [Ryoo and Das 2015] utilize the RFID reader frequency hopping and phase difference of signals to determine the distance between the reader antenna and the tag. They only use one or two linearly polarized directional antennas, but the tag must keep in stationary for at least ($\approx$ 2s) on 5 different channels. Wang *et al.* [Wang et al. 2015] is the first RF-based system that can accurately track the hand trajectory based on RF signals from a large number of antennas. RF-IDraw achieves good tracking accuracy with eight antennas connected to two RFID readers. Yet the dominant path may not exist in the effects of multipath interference, the performance of RF-IDraw is challenged. Yang *et al.* [Yang et al. 2015] proposed a hybrid probability model which combines PF with Weighted Centroid Localization (WCL) to achieve high accuracy and low computational cost, but there existed some limitations on the velocity. Yang *et al.* [Yang et al. 2015] demand a special RFID reader with a large number of tag arrays, which limits their application in some scenarios. Yang *et al.* [Yang et al. 2016] present an RFID-based solution, Tagbeat, to inspect mechanical vibration using COTS RFID tags and readers.

The above methods are somewhat not applicable in mobile cases, and we focus on leveraging the changing mobility profile for mobility detection. The intuition behind our design is that by analyzing the spatial-temporal dynamics in the mobility profiles, we can accurately estimate the mobility of tags. Previous work may rely on the reference tags or the dedicated hardware with many antennas to capture the mobility profile. Moreover, SAR-style techniques require constantly moving either the RFID reader or tags. In contrast, our scheme works on COTS devices with only two antennas in multipath-rich indoor environments.

6.3. Activity Recognition

Activity recognition solutions exploit the change of wireless signals incurred by the human's actions. RF-compass [Wang et al. 2013] presents a state-of-the-art WiFi-based interface, yet it only supports the detection and classification of a predefined set of nine gestures. WiVi [Adib and Katabi 2013] utilizes WiFi signals to detect users through walls and identify their gestures, which focuses on tracking through dense walls such as concrete by using MIMO interference nulling to eliminate reflections off static objects. RistQ [Parate et al. 2014] leverages the accelerations from a wrist strap to detect and recognize smoking gestures. RF-IDraw [Wang et al. 2015] can track human writing by tracking a passive RFID tag attached to his/her pen. E-eyes [Wang et al. 2014] is a location-oriented activity identification system, which leverages WiFi signals to recognize in-home human activities. Ding *et al.* [Ding et al. 2015] developed FEMO that uses the frequency shifts of the movements to determine what exercise a user is performing. In contrast, `i`^{2}`tag` can differentiate different levels of mobility using off-the-shelf RFID readers and tags.

7. CONCLUSION

In this paper, we have shown that existing mobile RFID solutions may suffer from serious performance degradation when the indoor environment is multipath-rich. Therefore, we have presented the architectural design of `i`^{2}`tag`, that can detect tag mobility and identify activities in typical indoor environments. `i`^{2}`tag` employs a novel *mobility profile* to quantify different levels of mobility, which seamlessly integrates RSSI variance and packet loss rate, as well as a relative-phase-based fingerprint. We have offered a *multiple dimensional dynamic time warping* algorithms to detect the tag mobility and utilize the multiclass SVMs algorithm to recognize human activities. A prototype has been implemented using a `Thingmagic` reader and `Impinj` tags and has been examined under various indoor environments. Experimental results have demonstrated its superiority in mobility detection and activity identification in various indoor environments.

8. ACKNOWLEDGMENTS

We would like to thank the anonymous reviewers for valuable and insightful comments. This research is supported in part by an NSERC Discovery Grant, a Strategic Project Grant, an E.W.R. Steacie Memorial Fellowship, and an Industrial Canada Technology Demonstration Program (TDP) grant.

REFERENCES

Fadel Adib and Dina Katabi. 2013. See through Walls with WiFi!. In *Proceedings of the ACM SIGCOMM 2013 Conference on SIGCOMM-SIGCOMM*, Vol. 13. Association for Computing Machinery, 12–16.

Jake K Aggarwal and Michael S Ryoo. 2011. Human activity analysis: A review. *ACM Computing Surveys (CSUR)* 43, 3 (2011), 16.

Muhammad Raisul Alam, Mamun Bin Ibne Reaz, and Mohd Alauddin Mohd Ali. 2012. A review of smart homespast, present, and future. *IEEE Transactions on Systems, Man, and Cybernetics, Part C (Applications and Reviews)* 42, 6 (2012), 1190–1203.

Paramvir Bahl and Venkata N Padmanabhan. 2000. RADAR: An in-building RF-based user location and tracking system. In *Proceedings of IEEE INFOCOM 2000*, Vol. 2. IEEE, 775–784.

Andreas Bulling, Ulf Blanke, and Bernt Schiele. 2014. A tutorial on human activity recognition using body-worn inertial sensors. *ACM Computing Surveys (CSUR)* 46, 3 (2014), 33.

Chih-Chung Chang and Chih-Jen Lin. 2011. LIBSVM: a library for support vector machines. *ACM Transactions on Intelligent Systems and Technology (TIST)* 2, 3 (2011), 27.

Jose M Chaquet, Enrique J Carmona, and Antonio Fernández-Caballero. 2013. A survey of video datasets for human action and activity recognition. *Computer Vision and Image Understanding* 117, 6 (2013), 633–659.

Krishna Chintalapudi, Anand Padmanabha Iyer, and Venkata N Padmanabhan. 2010. Indoor localization without the pain. In *Proceedings of the sixteenth annual international conference on Mobile computing and networking*. ACM, 173–184.

Han Ding, Longfei Shangguan, Zheng Yang, Jinsong Han, Zimu Zhou, Panlong Yang, Wei Xi, and Jizhong Zhao. 2015. Femo: A platform for free-weight exercise monitoring with rfids. In *Proceedings of the 13th ACM Conference on Embedded Networked Sensor Systems*. ACM, 141–154.

Abdelhamid Djouadi, Oe. Snorrason, and FD Garber. 1990. The quality of training sample estimates of the bhattacharyya coefficient. *IEEE Transactions on Pattern Analysis and Machine Intelligence* 12, 1 (1990), 92–97.

Joshua D Griffin and Gregory D Durgin. 2009. Complete link budgets for backscatter-radio and RFID systems. *IEEE Antennas and Propagation Magazine* 51, 2 (2009), 11–25.

Cory Hekimian-Williams, Brandon Grant, Xiuwen Liu, Zhenghao Zhang, and Piyush Kumar. 2010. Accurate localization of RFID tags using phase difference. In *2010 IEEE International Conference on RFID (IEEE RFID 2010)*. IEEE, 89–96.

Stefan Knerr, Léon Personnaz, and Gérard Dreyfus. 1990. Single-layer learning revisited: a stepwise procedure for building and training a neural network. In *Neurocomputing*. Springer, 41–50.

Manikanta Kotaru, Kiran Joshi, Dinesh Bharadia, and Sachin Katti. 2015. Spotfi: Decimeter level localization using wifi. In *ACM SIGCOMM Computer Communication Review*, Vol. 45. ACM, 269–282.

Xin Li, Yimin Zhang, and Moeness G Amin. 2009. Multifrequency-based range estimation of RFID tags. In *2009 IEEE International Conference on RFID*. IEEE, 147–154.

Tianci Liu, Lei Yang, Qiongzheng Lin, Yi Guo, and Yunhao Liu. 2014. Anchor-free backscatter positioning for rfid tags with high accuracy. In *IEEE INFOCOM 2014-IEEE Conference on Computer Communications*. IEEE, 379–387.

Robert Miesen, Fabian Kirsch, and Martin Vossiek. 2011. Holographic localization of passive uhf rfid transponders. In *2011 IEEE International Conference on RFID*. IEEE, 32–37.

Lionel M Ni, Yunhao Liu, Yiu Cho Lau, and Abhishek P Patil. 2004. LANDMARC: indoor location sensing using active RFID. *Wireless networks* 10, 6 (2004), 701–710.

Abhinav Parate, Meng-Chieh Chiu, Chaniel Chadowitz, Deepak Ganesan, and Evangelos Kalogerakis. 2014. Risq: Recognizing smoking gestures with inertial sensors on a wristband. In *Proceedings of the 12th annual international conference on Mobile systems, applications, and services*. ACM, 149–161.

Andreas Parr, Robert Miesen, and Martin Vossiek. 2013. Inverse sar approach for localization of moving rfid tags. In *RFID (RFID), 2013 IEEE International Conference on*. IEEE, 104–109.

Fabian Pedregosa, Gaël Varoquaux, Alexandre Gramfort, Vincent Michel, Bertrand Thirion, Olivier Grisel, Mathieu Blondel, Peter Prettenhofer, Ron Weiss, Vincent Dubourg, and others. 2011. Scikit-learn: Machine learning in Python. *Journal of Machine Learning Research* 12, Oct (2011), 2825–2830.

Low Level Reader Protocol. 2007. Version 1.0. 1. *EPCglobal Inc, Aug* (2007).

Anshul Rai, Krishna Kant Chintalapudi, Venkata N Padmanabhan, and Rijurekha Sen. 2012. Zee: zero-effort crowdsourcing for indoor localization. In *Proceedings of the 18th annual international conference on Mobile computing and networking*. ACM, 293–304.

Jihoon Ryoo and Samir R Das. 2015. Phase-based Ranging of RFID Tags with Applications to Shopping Cart Localization. In *Proceedings of the 18th ACM International Conference on Modeling, Analysis and Simulation of Wireless and Mobile Systems*. ACM, 245–249.

Stan Salvador and Philip Chan. 2007. Toward accurate dynamic time warping in linear time and space. *Intelligent Data Analysis* 11, 5 (2007), 561–580.

Moustafa Seifeldin, Ahmed Saeed, Ahmed E Kosba, Amr El-Keyi, and Moustafa Youssef. 2013. Nuzzer: A large-scale device-free passive localization system for wireless environments. *IEEE Transactions on Mobile Computing* 12, 7 (2013), 1321–1334.

Longfei Shangguan, Zheng Yang, Alex X Liu, Zimu Zhou, and Yunhao Liu. 2015. Relative localization of rfid tags using spatial-temporal phase profiling. In *12th USENIX Symposium on Networked Systems Design and Implementation (NSDI 15)*. 251–263.

Andrew Spielberg, Alanson Sample, Scott E Hudson, Jennifer Mankoff, and James McCann. 2016. RapID: A Framework for Fabricating Low-Latency Interactive Objects with RFID Tags. In *Proceedings of ACM CHI 2016 CHI Conference on Human Factors in Computing Systems*.

Chuyu Wang, Lei Xie, Wei Wang, Tao Xue, and Sanglu Lu. 2016. Moving tag detection via physical layer analysis for large-scale RFID systems. In *IEEE INFOCOM 2016-The 35th Annual IEEE International Conference on Computer Communications*. IEEE, 1–9.

Jue Wang, Fadel Adib, Ross Knepper, Dina Katabi, and Daniela Rus. 2013. RF-compass: robot object manipulation using RFIDs. In *Proceedings of the 19th annual international conference on Mobile computing & networking*. ACM, 3–14.

Jue Wang and Dina Katabi. 2013. Dude, where's my card?: RFID positioning that works with multipath and non-line of sight. *ACM SIGCOMM Computer Communication Review* 43, 4 (2013), 51–62.

Jue Wang, Deepak Vasisht, and Dina Katabi. 2015. RF-IDraw: virtual touch screen in the air using RF signals. *ACM SIGCOMM Computer Communication Review* 44, 4 (2015), 235–246.

Yan Wang, Jian Liu, Yingying Chen, Marco Gruteser, Jie Yang, and Hongbo Liu. 2014. E-eyes: device-free location-oriented activity identification using fine-grained WiFi signatures. In *Proceedings of the 20th annual international conference on Mobile computing and networking*. ACM, 617–628.

Carl Wong, Richard Klukas, and Geoffrey G Messier. 2008. Using WLAN infrastructure for angle-of-arrival indoor user location. In *Vehicular Technology Conference, 2008. VTC 2008-Fall. IEEE 68th*. IEEE, 1–5.

Jiang Xiao, Zimu Zhou, Youwen Yi, and Lionel M Ni. 2016. A Survey on Wireless Indoor Localization from the Device Perspective. *ACM Computing Surveys (CSUR)* 49, 2 (2016), 25.

Jie Xiong and Kyle Jamieson. 2013. ArrayTrack: a fine-grained indoor location system. In *Presented as part of the 10th USENIX Symposium on Networked Systems Design and Implementation (NSDI 13)*. 71–84.

Lei Yang, Jiannong Cao, Weiping Zhu, and Shaojie Tang. 2015. Accurate and efficient object tracking based on passive RFID. *IEEE Transactions on Mobile Computing* 14, 11 (2015), 2188–2200.

Lei Yang, Yekui Chen, Xiang-Yang Li, Chaowei Xiao, Mo Li, and Yunhao Liu. 2014. Tagoram: Real-time tracking of mobile RFID tags to high precision using COTS devices. In *Proceedings of the 20th annual international conference on Mobile computing and networking*. ACM, 237–248.

Lei Yang, Yao Li, Qiongzheng Lin, Xiang-Yang Li, and Yunhao Liu. 2016. Making sense of mechanical vibration period with sub-millisecond accuracy using backscatter signals. In *Proceedings of the 22nd Annual International Conference on Mobile Computing and Networking*. ACM, 16–28.

Lei Yang, Qiongzheng Lin, Xiangyang Li, Tianci Liu, and Yunhao Liu. 2015. See through walls with cots rfid system!. In *Proceedings of the 21st Annual International Conference on Mobile Computing and Networking*. ACM, 487–499.

Marwan Younis, Christian Fischer, and Werner Wiesbeck. 2003. Digital beamforming in SAR systems. *IEEE Transactions on Geoscience and Remote Sensing* 41, 7 (2003), 1735–1739.

Moustafa Youssef, Matthew Mah, and Ashok Agrawala. 2007. Challenges: device-free passive localization for wireless environments. In *Proceedings of the 13th annual ACM international conference on Mobile computing and networking*. ACM, 222–229.

Pengyu Zhang, Jeremy Gummeson, and Deepak Ganesan. 2012. Blink: A high throughput link layer for backscatter communication. In *Proceedings of the 10th international conference on Mobile systems, applications, and services*. ACM, 99–112.

Yiyang Zhao, Yunhao Liu, and Lionel M Ni. 2007. VIRE: Active RFID-based localization using virtual reference elimination. In *Proceedings of 2007 International Conference on Parallel Processing (ICPP 2007)*. IEEE, 56–56.

Liang Zhou. 2016. Mobile Device-to-Device Video Distribution: Theory and Application. *ACM Transactions on Multimedia Computing, Communications, and Applications (TOMM)* 12, 3 (2016), 38.